

Ultraluminous X-ray sources with flat-topped noise and QPO

Kirill Atapin,^{1,2*} Sergei Fabrika,^{2,3} Maria D. Caballero-García⁴

¹ *Sternberg Astronomical Institute, Moscow State University, Universitetsky pr., 13, Moscow, 119991, Russia*

² *Special Astrophysical Observatory, Nizhnij Arkhyz, 369167, Russia*

³ *Kazan Federal University, Kremlevskaya 18, Kazan 420008, Russia*

⁴ *Astronomical Institute, Academy of Sciences, Boční II 1401, CZ-14100 Prague, Czech Republic*

Submitted 2018 July 31.

ABSTRACT

We analyzed the X-ray power density spectra of five ultraluminous X-ray sources (ULXs) NGC 5408 X-1, NGC 6946 X-1, M 82 X-1, NGC 1313 X-1 and IC 342 X-1 that are the only ULXs which display both flat-topped noise (FTN) and quasi-periodic oscillations (QPO). We studied the QPO frequencies, fractional root-mean-square (rms) variability, X-ray luminosity and spectral hardness. We found that the level of FTN is anti-correlated with the QPO frequency. As the frequency of the QPO and brightness of the sources increase, their fractional variability decreases. We propose a simple interpretation using the spherization radius, viscosity time and α -parameter as basic properties of these systems. The main physical driver of the observed variability is the mass accretion rate which varies $\gtrsim 3$ between different observations of the same source. As the accretion rate decreases the spherization radius reduces and the FTN plus the QPO move toward higher frequencies resulting in a decrease of the fractional rms variability. We also propose that in all ULXs when the accretion rate is low enough (but still super-Eddington) the QPO and FTN disappear. Assuming that the maximum X-ray luminosity depends only on the black hole (BH) mass and not on the accretion rate (not considering the effects of either the inclination of the super-Eddington disc nor geometrical beaming of radiation) we estimate that all the ULXs have about similar BH masses, with the exception of M 82 X-1, which might be 10 times more massive.

Key words: accretion, accretion discs – X-rays: binaries – X-rays: individuals (NGC 5408 X-1, NGC 6946 X-1, M 82 X-1, NGC 1313 X-1, IC 342 X-1).

1 INTRODUCTION

Ultraluminous X-ray sources (ULXs) are bright, point-like, extra-galactic sources with observed X-ray luminosities $L_X \geq 10^{39}$ erg s⁻¹ (see Bachetti 2016; Kaaret et al. 2017, for a review). The nature of these objects is still unclear. The luminosities of ULXs exceed the Eddington limit for a typical stellar-mass black hole ($10 M_\odot$). Nevertheless they are not associated with galactic nuclei or background quasars. One of the possible models to explain their nature involves Intermediate Mass Black Holes (IMBHs) of 10^2 – $10^4 M_\odot$ with standard accretion discs (Colbert & Mushotzky 1999). This model implies that ULXs might be massive analogues of Galactic black hole binaries (BHBs). Another explanation is super-Eddington accretion onto stellar-mass black holes (Fabrika & Mescheryakov 2001; Poutanen et al.

2007). A key feature of the super-Eddington accretion predicted by numerical simulations (Ohsuga et al. 2005; Ohsuga & Mineshige 2011) is a strong optically thick wind, which covers the inner parts of the disc and collimates the radiation. In this case spectral and variability properties of ULXs could be different from BHBs (Gladstone et al. 2009) and resemble the superaccretor SS 433 in several aspects. In addition, the recent discovery of coherent X-ray pulsations in some sources (Bachetti et al. 2014; Fürst et al. 2016; Israel et al. 2017a,b) suggests that part of the whole population of ULXs are neutron stars accreting at super-Eddington rates (King et al. 2001, 2017; Middleton & King 2017).

SS 433 is the only known super-accretor in our Galaxy. It is a close binary system with a stellar-mass black hole (see Fabrika 2004 for a review). The accretion rate in this system is estimated to reach $300\dot{M}_{edd}$ (for the radiative efficiency of $\eta = 1/12$ and black hole mass $M_{BH} \approx 10 M_\odot$, Cherepashchuk et al. 2018), where \dot{M}_{edd} is the Eddington ac-

* E-mail: atapin.kirill@gmail.com

cretion rate. Optical spectra of SS 433 contain broad emission lines of hydrogen and He II with FWHM suggesting velocities of 1000 km/s originating from an accretion disc wind. The same line features have been revealed in the spectra from ULXs by Fabrika et al. (2015) from optical spectroscopy using the Subaru telescope. The latest showed that the optical spectra from ULXs are all very similar and resemble the optical spectrum from SS 433. This study shows that the lines present in the spectra support the idea of them arising from the wind funnel of a supercritical accretion disc instead from a donor-star wind or irradiated disc. Evidence of outflows have been suggested from X-ray spectral studies of NGC 5408 X-1, NGC 6946 X-1 (Middleton et al. 2014) and NGC 1313 X-1 (Middleton et al. 2015a). X-ray spectra from SS 433 have been studied by Fabrika et al. (2007) applying a model based on the spectra from ULXs. The X-ray spectral residuals show a big bump around ≈ 1 keV due to the difference between the neutral (N_H) and highly ionised absorption outflows. More recently, blue-shifted absorption lines with velocities of $\sim 0.2c$ were directly measured by Pinto et al. (2016) in the grating spectra of the same ULXs (see also Pinto et al. 2017; Kosec et al. 2018). These studies suggest the presence of highly ionized outflows in ULXs.

The X-ray spectra from ULXs have two common features: a soft excess below 2 keV and a roll-over at higher energies. The latter was initially discovered in *XMM-Newton* data (Stobbart et al. 2006; Gladstone et al. 2009). *NuSTAR* observations revealed an unambiguous high-energy cutoff above 10 keV (Bachetti et al. 2013; Walton et al. 2014). This spectral shape, hard to see in the case of BHBs, introduced the idea of a new, ‘ultraluminous’ accretion state (Roberts 2007; Gladstone et al. 2009). Depending on the ratio between the high- and low-energy parts of the spectrum, the ultraluminous state was splitted into three classes (Sutton et al. 2013): soft ultraluminous (SUL), hard ultraluminous (HUL) and broadened disc (BD). There is a trend for a particular source to belong to a specific class, although transitions between classes have also been observed (Pintore et al. 2014).

SS 433 is quite different from ULXs in X-rays. The apparent X-ray luminosity of this source is $\sim 10^{36}$ erg s $^{-1}$ due to the high inclination of its accretion disc ($i \gtrsim 60^\circ$). Nevertheless the bolometric luminosity is much higher and has been estimated to be $\sim 10^{40}$ erg s $^{-1}$ (Cherepashchuk 2002; Fabrika 2004; Middleton et al. 2018). The donor star in SS 433 contributes less than 15% of the whole luminosity. The observed X-ray spectrum of SS 433 is mostly due to emission from jets and also by reflection of the radiation coming from innermost parts of the disc on the funnel walls (Medvedev & Fabrika 2010). It has been suggested that, if being observed near face-on, SS 433 might resemble a ULX.

Examining the fast X-ray variability of SS 433 (Revnivtsev et al. 2006), it has been found that its power density spectrum is well-fitted by a broken power-law with a flat component ($P \propto f^0$) below 10^{-3} Hz (Atapin et al. 2015; Atapin & Fabrika 2016). This type of variability is similar to the flat-topped noise (hereafter FTN) observed in BHBs at the state of low accretion rate, i.e. ‘low/hard’ state (see McClintock & Remillard 2006; Belloni & Motta 2016 for reviews). However the standard states of black hole binaries do not correspond to what is typically observed in SS 433. Its spectral and variability behaviour depend on the precession

phase of the system which is fully determined by the visibility of the funnel of the supercritical accretion disc. The flat component in the PDS of SS 433 only emerges when the funnel is maximally opened to the observer. This suggests that the FTN can be produced by supercritical accretion as well.

Some ULXs also show FTN often accompanied by quasi-periodic oscillations (QPO). This is most clearly seen in NGC 5408 X-1 and M 82 X-1 which were the first ULXs where a QPO was discovered (Strohmayer & Mushotzky 2003; Strohmayer et al. 2007). The fact that both QPO and FTN appear together and the much lower frequency of the former compared to what has been usually seen in BHBs was initially considered as an evidence for the presence of an IMBH (Strohmayer & Mushotzky 2009; Dheeraj & Strohmayer 2012; Pasham & Strohmayer 2013). Recent studies using new data, in particular those regarding the discovery of the high-energy cutoff and the presence of an accelerated outflow, rule out the IMBH model, at least in the case of NGC 5408 X-1. Also it has been shown that the PDS of NGC 5408 X-1 does not appear to well match the type-C QPO observed in BHBs (Middleton et al. 2011). In the framework of super-Eddington accretion the observed variability properties of ULXs can be explained by the presence of an inhomogeneous wind (Middleton et al. 2011; Sutton et al. 2013; Middleton et al. 2015b).

QPOs have also been detected in NGC 6946 X-1 (Rao et al. 2010a), IC 342 X-1 (Agrawal & Nandi 2015), and in NGC 1313 X-1 (Pasham et al. 2015). The QPO in Ho IX X-1 reported by Dewangan et al. (2006) has not been confirmed in later studies (Heil et al. 2009). Despite a significant sample of ULXs with QPO, their properties have never been studied together. We notice that both QPO and FTN may appear at the same dataset and in some other observations the QPO/FTN may disappear. They are indeed connected features, as we will show in this work. Indeed, the main goal of this paper is to perform a joined analysis of the timing data from these ULXs. This procedure allows us to reveal any possible similarity in their variability properties and help us to understand the nature of the underlying physical processes driving it.

2 OBSERVATIONS

In this paper we analyse the short-term variability of five ULXs: NGC 5408 X-1, NGC 6946 X-1, M 82 X-1, NGC 1313 X-1 and IC 342 X-1. We used data from the *XMM-Newton* archive. All public observations longer than 10 ks have been included, excluding data sets affected by strong background flaring. We also excluded some observations of NGC 1313 X-1 where the source was positioned on the chip gap (this constitutes 1/4 of the whole dataset only). All the analysed data sets are listed in Table 1.

The observations were reduced using the *XMM-Newton* SAS version 15.0.0. We used the data from the European photon imaging camera (EPIC) pn and both MOS detectors. The first four observations of IC 342 X-1 were taken in ‘extended full-frame’ mode of the pn detector. All the other observations in Table 1 are in ‘full-frame’ imaging mode (time

Table 1. Log of the analyzed observations.

Obs. ID	Date	T_{obs}^a (ks)	T_{exp}^b (ks)	R_{net}^c (cnt/s)	Obs. ID	Date	T_{obs}^a (ks)	T_{exp}^b (ks)	R_{net}^c (cnt/s)
NGC 5408 X-1 ($D = 5.32$ Mpc ^d)									
0302900101 [†]	2006-01-13	132.2	90.0	0.538 ± 0.005	0653380401 [†]	2011-01-26	121.0	91.8	0.615 ± 0.005
0500750101 [†]	2008-01-13	115.7	72.6	0.542 ± 0.007	0653380501 [†]	2011-01-28	126.4	96.2	0.613 ± 0.005
0653380201 [†]	2010-07-17	128.9	76.5	0.691 ± 0.005	0723130301 [†]	2014-02-11	38.5	34.3	0.564 ± 0.009
0653380301 [†]	2010-07-19	130.8	104.7	0.672 ± 0.005	0723130401 [†]	2014-02-13	36.0	32.9	0.599 ± 0.010
NGC 6946 X-1 ($D = 6.72$ Mpc ^e)									
0200670301 [†]	2004-06-13	15.6	8.7	0.333 ± 0.014	0500730101 [†]	2007-11-08	31.9	25.7	0.306 ± 0.010
0500730201 [†]	2007-11-02	37.3	31.2	0.321 ± 0.009	0691570101 [†]	2012-10-21	119.3	97.4	0.386 ± 0.003
M82 X-1 ($D = 3.7$ Mpc ^f)									
0112290201 [†]	2001-05-06	30.5	22.0	7.38 ± 0.04	0560590301	2009-04-29	52.9	16.4	8.69 ± 0.07
0206080101 [†]	2004-04-21	104.3	56.1	5.89 ± 0.03	0657800101 [†]	2011-03-18	26.6	14.8	6.26 ± 0.03
0560590101	2008-10-03	31.9	25.5	13.63 ± 0.17	0657801901 [†]	2011-04-29	28.2	8.2	5.53 ± 0.04
0560181301	2009-04-03	27.3	9.2	7.92 ± 0.03	0657802101 [†]	2011-09-24	22.8	8.4	5.84 ± 0.03
0560590201	2009-04-17	44.6	12.5	11.55 ± 0.12	0657802301	2011-11-21	23.9	17.1	7.23 ± 0.07
NGC 1313 X-1 ($D = 3.88$ Mpc ^g)									
0106860101	2000-10-17	42.4	15.7	0.991 ± 0.008	0693850501 [†]	2012-12-16	125.2	96.4	1.141 ± 0.004
0150280601	2004-01-08	53.3	6.3	1.693 ± 0.022	0693851201 [†]	2012-12-22	125.2	86.3	1.173 ± 0.005
0205230601	2005-02-07	14.3	9.9	1.109 ± 0.016	0722650101	2013-06-08	30.7	15.6	1.156 ± 0.011
0405090101 [†]	2006-10-15	123.2	86.2	0.933 ± 0.004	0742590301	2014-07-05	63.0	60.0	2.106 ± 0.012
IC 342 X-1 ($D = 3.93$ Mpc ^h)									
0093640901	2001-02-11	10.9	5.9	0.738 ± 0.015	0206890401	2005-02-10	23.9	5.3	2.25 ± 0.03
0206890101	2004-02-20	23.9	13.9	1.77 ± 0.05	0693850601 [†]	2012-08-11	59.9	37.2	0.835 ± 0.015
0206890201	2004-08-17	23.9	19.6	0.862 ± 0.007	0693851301	2012-08-17	60.1	35.3	1.029 ± 0.023

Notes. ^aThe total observation time. ^bUseful exposure time after removing background flares. ^cNet pn+MOS1+MOS2 count rate in the 1–10 keV band. ^dDistance to the host galaxy is taken from Tully et al. (2013). ^eTikhonov (2014). ^fMedian value of the distance from NED (<http://ned.ipac.caltech.edu>). ^gTikhonov & Galazutdinova (2016). ^hTikhonov & Galazutdinova (2010). [†]QPO was detected in this observation.

resolution is 73.4 ms and 2.6 s for pn and MOS¹ respectively). The data sets were filtered with patterns 0–4 for pn and 0–12 for MOS including only single and double pixel events and applying ‘FLAG==0’ to exclude the events from bad pixels and events near chip gaps.

Particular attention was taken removing background flares because of the spurious variability introduced by flaring may distort the power spectra. First of all, we extracted pn light curves from the entire field of view in the 10–12 keV band. The count rate of non-flaring background have proven to be slightly different between the observations. For most data sets we applied the standard screening criterion² including only time periods where the pn count rate was not higher than 0.4 count s⁻¹. However we found that for some observations with stable background this threshold rejects too many good data points. In these cases we used a less restrictive condition and included time periods where the count rate was not higher than three times the standard deviations from the mean.

The flux from M82 X-1 is significantly contaminated by diffuse emission from the host galaxy and by another bright

ULX — M82 X-2. The separation between X-1 and X-2 is only 5” (Matsumoto et al. 2001), which is near the limit of the *XMM-Newton* spatial resolution. Both ULXs are highly variable and have about similar luminosities. We were not able to avoid this contamination, however, below we discuss how it can affect the results of our analysis (Sec. 3.2).

Source light curves were extracted from circular regions with a radius of 32”. For M82 X-1 we additionally used smaller aperture of 12” radius to reduce the contribution of the emission from the host galaxy, and compared the results obtained from both apertures. For all the sources except M82 X-1 which cannot be resolved as a separate point source, the circle position was adjusted to be centred around the brightest pixel in each observation. In the case of M82 X-1 the centre of the region was fixed at RA = 09 55 50.2, Dec = +69 40 47 (Matsumoto et al. 2001). Background regions were chosen to be as large as possible to diminish statistical fluctuations, located in the same chip of the source in areas free of other sources and away from the read-out direction. Light curves were extracted with the task EVSELECT with the same bin-size for all the detectors. To prevent possible asynchronicity between pn and MOS light curves, we launched this task with parameters ‘timemin’ and ‘timemax’ (Barnard et al. 2007) assigning the same start and stop time for each detector. Background light curves were subtracted using the task EPICLCCORR, which takes into account instrumental effects like vignetting, bad pixels, etc. Then we

¹ Resolution of the MOS1 has been reduced to 2.7 s for observations after December 2012:

<https://www.cosmos.esa.int/web/xmm-newton/mos1-ccd3>

² <https://www.cosmos.esa.int/web/xmm-newton/sas-thread-epic-filterbackground>

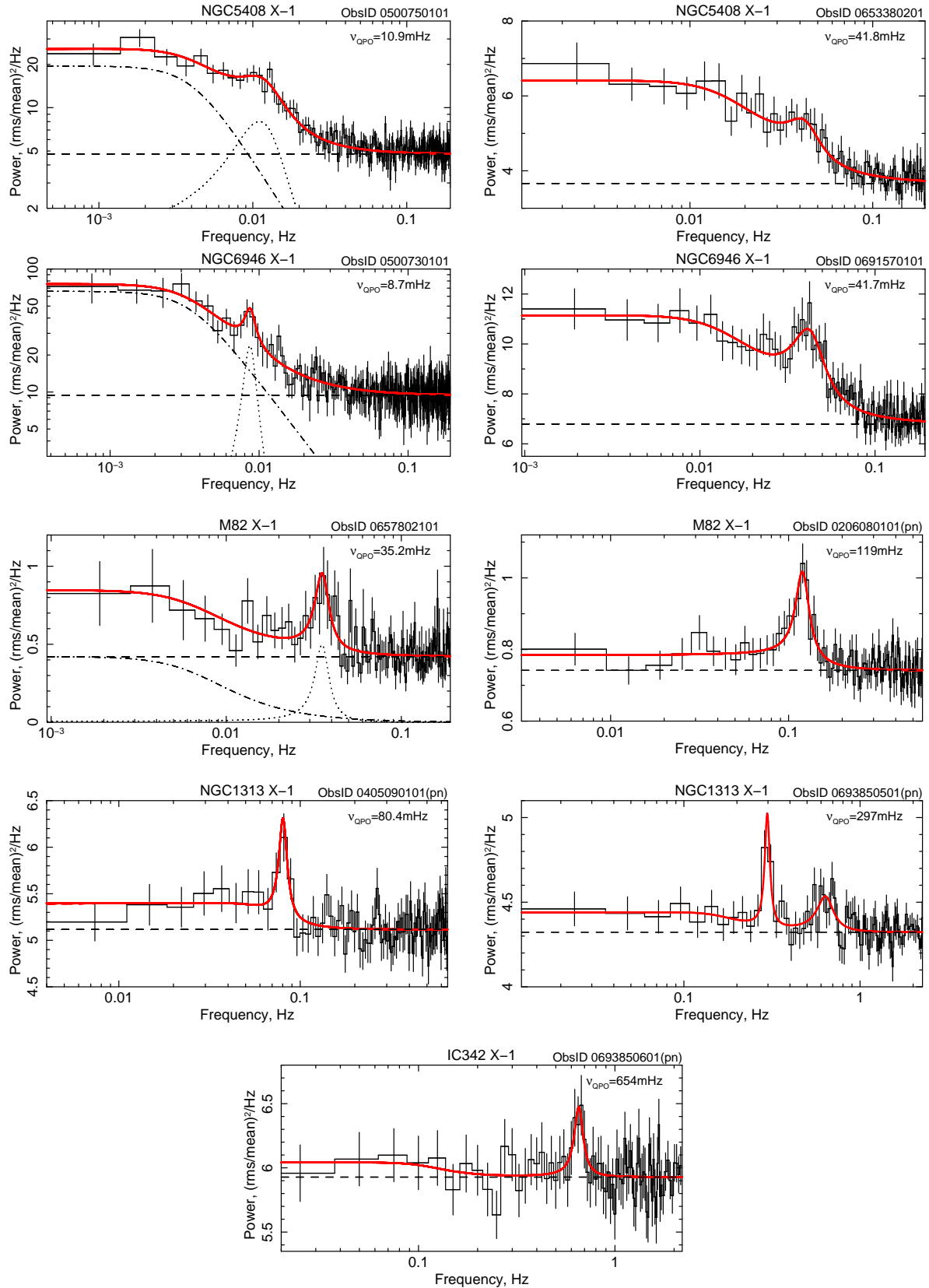


Figure 1. Power density spectra of five ULXs that were reported to exhibit QPO (energy band of 1–10 keV). The observations with the lowest and the highest QPO frequency for each source are shown on the left-hand and right-hand sides respectively. The level of Poisson noise is shown by dashed lines. The solid lines are the best-fitting models, the dotted and dash-dotted lines represent model components: Lorentzians and broken power law (these components have much lower levels than Poisson noise in most cases and are well below the lower boundaries of the plots). It is clearly seen that a lower QPO centroid frequency corresponds to a higher power in the PDS above Poisson noise.

Table 2. Best fitting model parameters for the PDS in which we detected QPO.

Obs. ID	f_q^a mHz	W_q^b mHz	Q^c	R_q^d (rms/mean) ²	f_b^e mHz	β^f	A^g	χ^2/dof	S_b^h σ	S_q^i σ
NGC 5408 X-1										
0500750101	$10.9^{+1.5}_{-2.9}$	9^{+6}_{-4}	1.2	$10^{+9}_{-5} \cdot 10^{-2}$	$4.1^{+2.4}_{-1.6}$	> 1.35	19^{+5}_{-3}	231.7/201	5.2	3.4
0723130301	$11.9^{+2.1}_{-1.7}$	10^{+3}_{-4}	1.2	$12.9^{+2.4}_{-7.1} \cdot 10^{-2}$	$4.8^{+1.6}_{-1.3}$	> 1.64	15^{+4}_{-3}	230.6/210	5.0	3.3
0723130401	$13.9^{+1.1}_{-0.9}$	5^{+5}_{-3}	2.8	$6^{+4}_{-4} \cdot 10^{-2}$	7^{+6}_{-3}	$1.54^{+0.7}_{-0.4}$	$11.7^{+2.6}_{-2.2}$	142.2/162	5.3	3.0
0302900101	$18.1^{+2.1}_{-2.0}$	20^{+5}_{-6}	0.9	$13.3^{+2.4}_{-5.9} \cdot 10^{-2}$	$5.9^{+1.5}_{-1.9}$	> 1.26	$7.8^{+2.4}_{-1.5}$	152.0/155	4.9	5.1
0653380501	$18.2^{+2.3}_{-3.1}$	19^{+6}_{-7}	1.0	$11^{+5}_{-5} \cdot 10^{-2}$	$6.5^{+2.7}_{-2.0}$	> 1.29	$7.3^{+1.8}_{-1.7}$	117.2/113	5.1	4.1
0653380401	$18.7^{+1.9}_{-2.2}$	20^{+4}_{-5}	0.9	$10.8^{+2.7}_{-3.5} \cdot 10^{-2}$	$5.6^{+1.2}_{-1.7}$	> 1.48	$5.6^{+1.2}_{-1.2}$	172.1/169	4.3	4.0
0653380301	$39.3^{+2.7}_{-3.2}$	22^{+15}_{-11}	1.8	$3.6^{+3.5}_{-2.4} \cdot 10^{-2}$	18^{+7}_{-7}	> 1.02	$2.5^{+0.6}_{-0.5}$	69.8/63	3.7	3.0
0653380201	$41.8^{+2.8}_{-9.8}$	22^{+27}_{-16}	1.9	$3.3^{+6.1}_{-2.4} \cdot 10^{-2}$	19^{+10}_{-8}	> 0.96	$2.5^{+0.7}_{-0.7}$	59.2/73	3.7	3.0
NGC 6946 X-1										
0500730101	$8.7^{+0.8}_{-0.9}$	$1.6^{+2.2}_{-1.1}$	5.4	$6^{+8}_{-4} \cdot 10^{-2}$	$3.4^{+1.4}_{-1.2}$	$1.58^{+0.28}_{-0.25}$	66^{+20}_{-16}	326.4/247	3.5	2.8
0500730201	$9.4^{+1.1}_{-0.9}$	$5.2^{+3.4}_{-2.2}$	1.8	$14^{+9}_{-6} \cdot 10^{-2}$	$2.2^{+1.6}_{-1.3}$	$1.26^{+0.6}_{-0.3}$	45^{+24}_{-14}	286.8/292	3.2	3.3
0200670301	27^{+5}_{-4}	$5.2^{+3.4}_{-1.3}$	5.2	$6^{+4}_{-4} \cdot 10^{-2}$	$12.0^{+2.7}_{-3.7}$	> 1.33	11^{+4}_{-3}	80.0/77	3.6	2.6
0691570101	$41.7^{+2.4}_{-3.7}$	23^{+16}_{-10}	1.8	$9^{+8}_{-5} \cdot 10^{-2}$	16^{+9}_{-5}	> 0.86	$4.1^{+1.2}_{-1.0}$	78.0/93	6.1	3.4
M82 X-1										
0657802101	$35.2^{+1.9}_{-2.4}$	$7.9^{+4.7}_{-2.8}$	4.5	$6.0^{+2.8}_{-2.5} \cdot 10^{-3}$	7^{+3}_{-3}	$1.42^{+1.2}_{-0.7}$	$0.42^{+0.14}_{-0.14}$	97.4/94	2.6 (3.7)	3.3
0657801901	$46.2^{+1.9}_{-3.0}$	9^{+6}_{-5}	5.1	$9^{+4}_{-4} \cdot 10^{-3}$	27^{+20}_{-14}	> 1.18	$0.15^{+0.7}_{-0.7}$	84.2/75	2.9 (3.2)	3.5
0657800101	$47.0^{+2.2}_{-2.2}$	8^{+7}_{-5}	5.8	$4.5^{+2.4}_{-2.4} \cdot 10^{-3}$	11^{+5}_{-5}	> 0.89	$0.27^{+0.26}_{-0.10}$	55.0/42	2.2 (3.5)	2.9
0112290201	$52.7^{+3.7}_{-2.6}$	15^{+11}_{-7}	3.5	$3.6^{+1.8}_{-1.4} \cdot 10^{-3}$	8.9^{+12}_{-5}	> 1.13	$0.22^{+0.11}_{-0.08}$	70.7/70	2.7 (4.6)	3.9
0206080101	119^{+3}_{-5}	26^{+19}_{-12}	4.57	$9.9^{+5}_{-2.9} \cdot 10^{-3}$	110^{+90}_{-80}	> 0.35	$0.039^{+0.023}_{-0.025}$	66.3/82	1.3 (2.5)	6.2
NGC 1313 X-1										
0405090101	$80.4^{+2.9}_{-2.2}$	10^{+6}_{-5}	8.0	$1.7^{+0.9}_{-1.1} \cdot 10^{-2}$	60^{+40}_{-30}	> 0.96	$0.28^{+0.16}_{-0.07}$	133.2/131	1.3 (2.4)	3.2
0693851201	268^{+21}_{-15}	70^{+65}_{-50}	3.8	$4.2^{+3.0}_{-2.2} \cdot 10^{-2}$	< 130	> 0.65	$0.27^{+0.41}_{-0.09}$	40.0/55	1.3 (2.3)	3.6
0693850501 ^j	297^{+5}_{-6}	24^{+30}_{-22}	12.4	$2.9^{+1.4}_{-1.5} \cdot 10^{-2}$	< 350	> 0.74	$0.11^{+0.08}_{-0.06}$	54.5/66	1.2 (2.1)	4.4
	630^{+60}_{-40}	80^{+100}_{-50}	7.8	$5.3^{+3.1}_{-2.8} \cdot 10^{-2}$	< 350	> 0.74	$0.11^{+0.08}_{-0.06}$	54.5/66	1.2 (2.1)	2.7
IC 342 X-1										
0693850601	654^{+26}_{-30}	80^{+70}_{-50}	8.2	$7^{+11}_{-3} \cdot 10^{-2}$	< 320	> 0.51	< 0.29	43.3/73	< 1 (1.2)	3.2

Note. The data sets are ordered by the centroid frequency of the QPO. All uncertainties refer to 90% confidence level. ^aCentroid frequency of the QPO. ^bFWHM of the QPO. ^cQuality factor of the QPO $Q = f_q/W_q$. ^dTotal power under the QPO profile. ^eBreak frequency of the flat-topped noise (FTN). ^fPower-law index above the break. ^gLevel of the FTN (in units of (rms/mean)² Hz⁻¹). ^hStatistical significance of the flattening of power spectrum at lower frequencies and also significance of the presence of any power besides QPO above the Poisson noise (shown in brackets) obtained via F-test. ⁱStatistical significance of the QPO obtained via F-test. ^jTwo Lorentzians were used to fit this observation.

created combined pn+MOS1+MOS2 light curves for all the observations.

3 TIMING ANALYSIS

3.1 Power spectra

Studies of the power spectra of NGC 5408 X-1 (Dheeraj & Strohmayer 2012; Caballero-García et al. 2013a) and M 82 X-1 (Pasham & Strohmayer 2013; Caballero-García et al. 2013b) have shown that the properties of the QPO vary between different observations. Sometimes in M 82 X-1 the QPO disappears. So, first of all, we examined all the data sets to check for the presence of the QPO and make a preliminary estimate of its centroid frequency. In order to increase the signal we started producing the PDS from combined pn+MOS light curves that covered frequencies up to the Nyquist frequency of $f_{nq} \approx 0.2$ Hz. If the QPO peak was absent in this frequency range, we produced a pn-only PDS, which allowed to extend the frequency range up to $f_{nq} \approx 6.8$ Hz. Eventually, QPOs

have been detected in 21 data sets of 36 and are listed in Table 1. We have analyzed all the observations with QPO from NGC 5408 X-1 and NGC 6946 X-1, five observations from M 82 X-1, three from NGC 1313 X-1 and only one observation from IC 342 X-1. We explored the PDS of these observations in more detail. However the failure to detect QPO in the rest of PDS might still be caused by insufficient length of those observations.

The PDS were constructed as follows. Since the fast X-ray variability of ULXs is stronger at higher energies (Middleton et al. 2011; De Marco et al. 2013), we used light curves in the energy band of 1–10 keV. To increase the signal-to-noise ratio, we divided the light curves into shorter segments of equal length, produced individual power spectra from each segment and averaged them out. The length of the segments was chosen separately for each observation to make the lowest frequency in the resultant PDS be around one tenth – one fiftieth of the QPO frequency. Some segments had gaps resulting from the background flaring removing and telemetry dropouts. We rejected such segments when the fraction of the gaps was greater than 5% of the

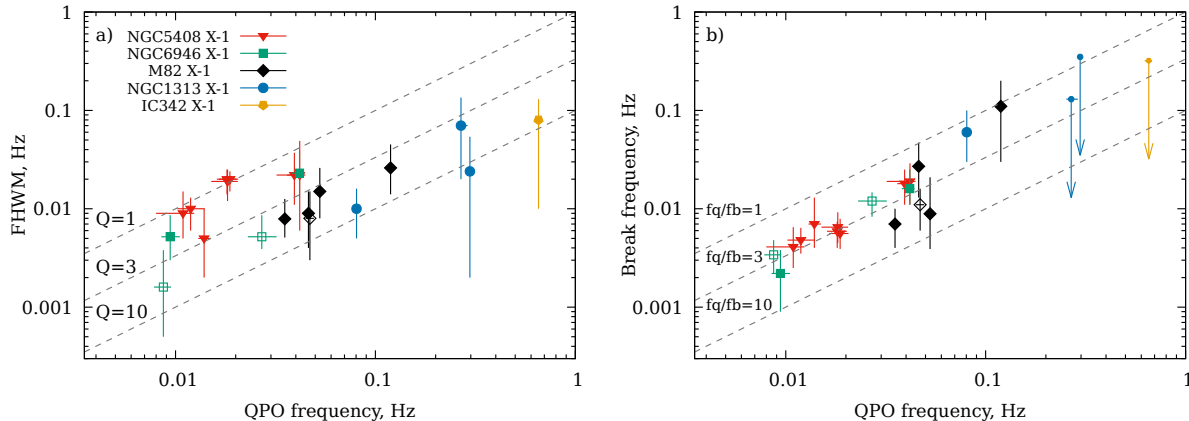


Figure 2. *Left panel:* The FWHM of the QPO as a function of its centroid frequency. The dashed lines correspond to constant quality factors $Q = f_q/W_q = 1, 3$ and 10 . *Right panel:* The QPO centroid frequency versus the break frequency of the flat-topped noise. Arrows denote observations where we obtained only the upper limit of f_b (Table 2). The dashed lines represent ratios $f_q/f_b = 1, 3$ and 10 . We found mean $f_q/f_b \approx 3$. Unfilled data points denote QPO with significance less than 3σ (observations of NGC 6946 X-1 and M 82 X-1).

length of the segments. Otherwise the gaps were filled with values of the count rates having a normal distribution with the same mean and rms as the original time series. Then the PDS were normalized to the fractional rms squared normalization (van der Klis 1997; Vaughan et al. 2003a). The PDS with the lowest and the highest QPO frequencies for each source are shown in Fig. 1.

All the PDS in which we detected QPO have a similar structure. The power increases towards lower frequencies as a power law and bends to the flat spectrum $P \propto f^0$ (FTN) near the break frequency f_b . The QPO peak is located on the power-law part of the PDS close to the break. At the highest frequencies the power spectrum is dominated by Poisson noise.

The PDS were fitted using XSPEC version 12.9.0i with a model consisting of three components. The QPO peak was approximated by a Lorentzian with a centroid frequency f_q , FWHM width W_q and the total area under the Lorentzian R_q . To describe the continuum we used a broken power law

$$P \propto \frac{A}{f^{\beta_0} \sqrt{1 + (f/f_b)^{2\beta}}}, \quad (1)$$

with index β above the break and β_0 fixed at zero to represent the white noise below the break. The normalization of this model was chosen so that A was the level of the flat component. Poisson noise was modelled by a constant which was allowed to vary. The obtained model parameters are shown in Table 2.

For each PDS, we estimated the statistical significance of the QPO using the F-test. However, it has been noted that the classical F-test may give an incorrect result in the case of testing for the presence of additive model components like QPO in PDS or emission lines in energy spectra (Protassov et al. 2002) because the test statistic may not follow the Fisher distribution. Additional procedures are needed to calibrate the test statistic. Therefore, for each data set we performed simulations as proposed by Protassov et al. (2002). First of all, we fitted each observed PDS by two models: the model described above (target model) and the continuum-only model (null model). All the model parameters (including the QPO and break frequen-

cies) were allowed to vary. For both models, we obtained the χ^2 and computed the *observed F-statistic* via standard formulae accounting for the difference in the number of degrees of freedom between the two models. Then for each data set we simulated 10 000 PDS according to the null model with parameters fixed at their best-fit values using the XSPEC command ‘fakeit’ (to obtain the Gaussian errors in the simulated PDS we made sure that the POISSERR keyword in the FITS header is set to “false”) and fitted them in the same way to obtain the *simulated F-statistic*. Comparing the F-statistics for the simulated data with the observed one, we obtained the p-value (probability that the observed PDS could be properly fitted without the Lorentzian model component). Eventually, we have found that the p-values derived from simulations and inferred from the Fisher distribution (classical F-test) are consistent with each other within 30% in all the cases³. For clarity, in Table 2 the p-values are converted to sigmas.

Similar simulations were carried out to test the significance of the FTN. As a null model we used one consisting of a power law (without break), Lorentzian and a constant for the Poisson noise. The probabilities obtained via F-test (Table 2) suggest that only NGC 5408 X-1 and NGC 6946 X-1 show strong evidence of a break. The significances of the breaks in M 82 X-1, NGC 1313 X-1 and IC 342 X-1 are much lower. This is largely due to the strong Poisson noise which dominates over the intrinsic variability of these sources and does not allow to constrain the shape of their PDS continua. Thus, for these sources we additionally tested the presence of any variability present in the continuum. In this case, as a null model we used ‘Lorentzian+constant’ and performed simulations similar to those described above. The obtained probabilities converted to sigmas are provided in the same column of Table 2 but in brackets.

Our measurements of the QPO centroid frequencies are consistent with the results obtained by other authors (NGC 5408 X-1 – Dheeraj & Strohmayer

³ Due to the limited sample, the simulations cannot reveal p-values less than $1 \cdot 10^{-4}$ ($\sigma \approx 3.9$).

2012; Caballero-García et al. 2013a; De Marco et al. 2013; NGC 6946 X-1 – Rao et al. 2010a; M 82 X-1 – Pasham & Strohmayer 2013; Caballero-García et al. 2013b; NGC 1313 X-1 – Pasham et al. 2015; IC 342 X-1 – Agrawal & Nandi 2015) for all the observations except ObsID 0657802301 of M 82 X-1. We did not detect any QPO in this observation whilst Pasham & Strohmayer (2013) reported one at $f_q \approx 0.2$ Hz. Also we have not found evidence for a second highly significant QPO peak in any observation except ObsID 0693850501 (NGC 1313 X-1). In the latter case, we placed the second Lorentzian near 0.6 Hz (Fig. 1) improving the χ^2 from 65.4/69 to 54.5/66, however, this improvement is still insufficient to consider it as a firm detection ($\sigma \approx 2.7$). For ObsID 0657800101 (M 82 X-1) we obtained the QPO significance $\sigma \approx 2.9$. Nevertheless, we included this observation in further analysis because it has already been studied by Pasham & Strohmayer (2013) and Caballero-García et al. (2013b) who estimated its significance as 3.9 and 3.6, respectively. We also included two observations of NGC 6946 X-1: ObsID 0500730101 (analysed by Rao et al. 2010a) and ObsID 0200670301, obtaining $\sigma \approx 2.8$ and 2.6, respectively. This level should be considered only as a marginal detection, therefore we marked these data sets in the figures below.

For M 82 X-1 we produced PDS taken from 32" and 12" radius apertures and found that the QPO properties are similar in both cases. In Table 2 we prefer to present the model parameters from the PDS for the 32" -radius because they are more stable and have lower uncertainties. The spectral index β turned out to be poorly constrained for most of the observations, since the power-law portion in the PDS near the QPO is better described by the wing of the Lorentzian than by the broken power law. We therefore provide only lower limits of β for most of the PDS in Table 2.

The QPO frequencies, considering the sample of five sources as a whole, vary in a broad range spanning about two orders of magnitude. The lowest frequency is seen in NGC 6946 X-1 (9.4 mHz, or 8.7 mHz taking into account ObsID 0500730101 with marginally detected QPO) and the highest in IC 342 X-1 (654 mHz). However, each source shows variations of f_q by a factor of 3–5. In Fig. 2a we plot the QPO centroid frequency versus the FWHM of the QPO peak. The quality factors of the QPO ($Q = f_q/W_q$) in NGC 5408 X-1 and in two observations of NGC 6946 X-1 are about unity, which is lower than usually assumed for QPO ($Q \gtrsim 2$). Other authors reported similar values (within errors) in these observations (Pasham & Strohmayer 2013; De Marco et al. 2013; Rao et al. 2010a). The rest of ULXs showed higher quality factors ($Q \sim 3 - 10$).

The break in the PDS moves together with the QPO peak frequency between different observations keeping the ratio f_q/f_b nearly constant (within uncertainties). For NGC 5408 X-1, NGC 6946 X-1 and M 82 X-1 we obtained the mean $f_q/f_b \approx 3$ (Fig. 2b, however, in the case of M 82 X-1 the shape of the continuum is not well-constrained). In sub-Eddington BHs this ratio is about 10 (Wijnands & van der Klis 1999), i.e. the QPO peak is located much farther from the break. It has been noted by Middleton et al. (2011) that such a discrepancy may suggest a difference in the accretion states between BHs and ULXs.

Table 3. Fractional rms variability (including contribution from both FTN and QPO) in the 0.001–0.2 Hz frequency range.

Obs. ID	F_{rms}	Obs. ID	F_{rms}
NGC 5408 X-1			
0302900101 [†]	0.445 ± 0.009	0653380401 [†]	0.404 ± 0.010
0500750101 [†]	0.489 ± 0.014	0653380501 [†]	0.405 ± 0.008
0653380201 [†]	0.317 ± 0.012	0723130301 [†]	0.454 ± 0.017
0653380301 [†]	0.329 ± 0.010	0723130401 [†]	0.451 ± 0.015
NGC 6946 X-1			
0200670301 [†]	0.43 ± 0.07	0500730101 [†]	0.65 ± 0.04
0500730201 [†]	0.63 ± 0.04	0691570101 [†]	0.412 ± 0.016
M 82 X-1			
0112290201 [†]	0.063 ± 0.008	0560590301	0.034 ± 0.008
0206080101 [†]	0.089 ± 0.005	0657800101 [†]	0.098 ± 0.006
0560590101	0.015 ± 0.008	0657801901 [†]	0.107 ± 0.016
0560181301	0.040 ± 0.012	0657802101 [†]	0.110 ± 0.011
0560590201	0.025 ± 0.009	0657802301	0.036 ± 0.009
NGC 1313 X-1			
0106860101	0.123 ± 0.023	0693850501 [†]	0.093 ± 0.011
0150280601	0.051 ± 0.026	0693851201 [†]	0.100 ± 0.010
0205230601	0.13 ± 0.04	0722650101	0.12 ± 0.03
0405090101 [†]	0.148 ± 0.012	0742590301	0.035 ± 0.011
IC 342 X-1			
0093640901	0.13 ± 0.05	0206890401	0.029 ± 0.022
0206890101	0.06 ± 0.03	0693850601 [†]	0.082 ± 0.016
0206890201	0.069 ± 0.016	0693851301	0.06 ± 0.03

Note. The data sets are ordered in the same way as in Table 1. [†]QPO was detected in this observation.

3.2 Correlations between the QPO frequency, fractional variability and luminosity

De Marco et al. (2013) have revealed a relation between the centroid frequency of the QPO and variability of the source when analyzing six long observations of NGC 5408 X-1. The total amount of power in the PDS decreases as the QPO frequency increases. We found that the same is true for all the five ULXs from our sample (Fig. 1). The anti-correlation between the FTN level and the QPO centroid frequency is seen in Table 2 (parameters A and f_q respectively, at least for NGC 5408 X-1, NGC 6946 X-1 and M 82 X-1 where the flat components are highly significant). Parameter A has a low accuracy due to high uncertainties of the PDS at the lowest frequencies.

For all the observations we calculated the fractional rms variability (F_{rms} , Edelson et al. 2002; Vaughan et al. 2003a) as a more accurate measure of the intrinsic variability of the source. Being an integral quantity, F_{rms} does not depend on the specific shape of the PDS and expresses the total source variability within a certain frequency range. It is insensitive to the model uncertainties and can be obtained also for those PDS where we were unable to constrain the shape of the continuum. The fractional variability is defined as the root mean square of the light curve corrected by the effects of random-noise measurements and normalized to the mean source count rate.

To ensure uniformity we obtained F_{rms} from the 1000 sec length segments of combined pn+MOS light curves

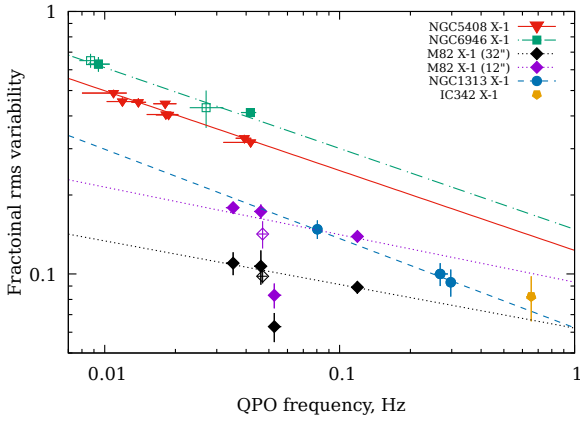


Figure 3. Fractional rms variability in the frequency range of 0.001 – 0.2 Hz in the 1–10 keV energy band as a function of the best fit QPO centroid frequency. For M82 X-1 we show the fractional rms variability taken from both 32" and 12" radius apertures. Lines of different types represent the power-law fits to the data point of different source. Unfilled data points denote QPO with significance less than 3σ (Table 2).

(this corresponds to the frequency range of 10^{-3} – 0.2 Hz) for every observation regardless the QPO frequency. Such relatively long segments were chosen in order to include, at least in part, variability at frequencies below the break. Since the number of segments goes from 6 (in the worst case) to ~ 100 , we were able to compute the sample mean and its standard deviation. Results are presented in Table 3.

In Fig. 3 we present the fractional variability as a function of the QPO centroid frequency. The F_{rms} (including contributions from both the continuum and QPO) is observed to decrease as the QPO frequency increases in all the cases. A power law fitting these data $F_{rms} \propto f_q^{-\gamma}$ yields $\gamma = 0.31 \pm 0.03$ ($1-\sigma$ error) for NGC 5408 X-1 and NGC 6946 X-1. For NGC 1313 X-1 we obtained a similar index $\gamma = 0.34 \pm 0.03$ but the variability level shown by this source is significantly lower.

Although in the fractional variability both QPO and FTN contribute, we note that the observed negative correlation is provided mainly by the FTN, whose level monotonically and rapidly drops as the QPO frequency increases (Table 2). At the same time, variations of the power due to the QPO peak appear to be random (parameter R_q in Table 2).

M82 X-1 stands out from the other sources. It shows a shallower slope $\gamma = 0.17 \pm 0.05$ for 32" aperture (and 0.18 ± 0.12 for 12") and a lower variability level. We suppose that such a difference may be due to the contamination of the source flux by diffuse emission from the host galaxy and neighbouring sources. This emission being less variable may ‘dilute’ the source variability. This idea is confirmed by the difference between the F_{rms} values obtained from 32" and 12" radius apertures. In the case of a single isolated source, the fractional variability would not depend on the aperture size, since the absolute rms is in the numerator and the mean count rate is in the denominator change proportionally. But in the figure one can see that the smaller aperture gives higher F_{rms} values because it collects less of the contaminating emission.

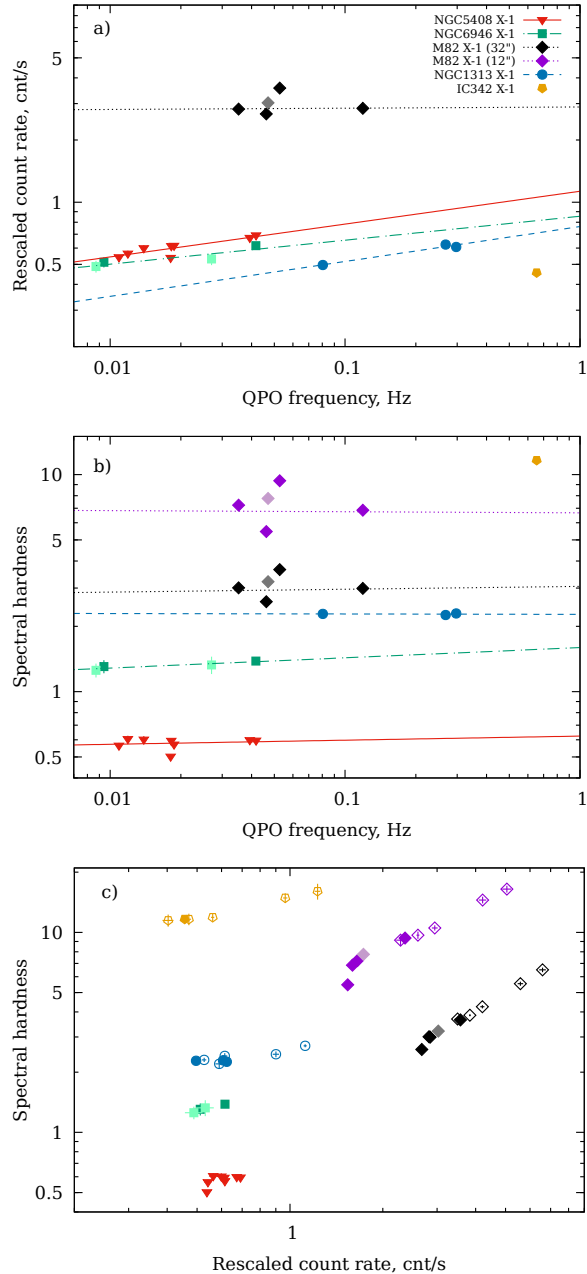


Figure 4. Count rate in the 1–10 keV band (*top panel*) and hardness ratio between the 1-10 keV and 0.3-1 keV bands (*middle panel*) against the QPO frequency, and hardness against count rate (*bottom panel*). To account the difference in distances to the ULX host galaxies, the count rates were rescaled to the distance of NGC 5408. Observations of NGC 6946 X-1 and M 82 X-1 where the significance of the QPO is less than 3σ (Table 2) are shown by lighter colours. Observations where we did not detect QPO are indicated by unfilled data points. Error bars (comparable to the point size) represent only intrinsic errors of the count rates, uncertainties of the distances are not included. Error bars of the QPO frequencies are omitted.

By taking a smaller aperture in M82 X-1, one can reduce only the contamination by diffuse emission from the host galaxy. However much of the contaminating flux comes from the ULX pulsar M82 X-2. Sources X-1 and X-2 are only marginally resolvable by MOS detectors and completely unresolvable by pn. Pasham & Strohmayer (2013) carried out surface brightness modelling of the MOS images from the same five *XMM-Newton* observations we present here, and compared the luminosities of both ULXs. They found that X-2 was twice brighter than X-1 during the observation ObsID 0112290201 (the lowest data point in Fig. 3, that we excluded from the fit) and was fainter by a factor of 1.5–2 during the rest of observations. Since both sources are highly variable, Feng & Kaaret (2007) and Pasham & Strohmayer (2013) analysed the PDS from different areas near X-1 and X-2 in order to distinguish which source is the origin of the QPO. It has been confirmed that the QPO peak observed above 30 mHz is produced by M82 X-1. Source X-2 also showed a QPO-like feature near 3 mHz but, above 10 mHz, its power spectrum is dominated by Poisson noise (Feng et al. 2010). Thus, taking into account the contamination from both the diffuse emission of the galaxy and M82 X-2, we conclude that the true location of M82 X-1 in Fig. 3 should be between NGC 5408 X-1 and NGC 1313 X-1, i.e. 2–3 times higher than it already is.

In Fig. 4a and Fig. 4b we show the source count rate and spectral hardness as a function of the QPO centroid frequency. To be able to compare the luminosities of the ULXs located in different galaxies, we rescaled the count rates to the distance of NGC 5408 X-1 (the distances to the host galaxies are provided in Table 1). Nevertheless, it should be noted that the (corrected) count rate (hereafter called apparent luminosity) represents only a fraction of the real (intrinsic) luminosity because it depends on a particular shape of the source spectrum and also does not account for possible beaming and absorption column which differs between sources and also can change over time (Middleton et al. 2015a). An increasing trend of the source apparent luminosity with the QPO frequency is seen in the figure. However this trend is relatively weak: if the frequency increases by ten times, the count rate changes by 40% only. We obtained power-law slopes of 0.16 ± 0.04 for NGC 5408 X-1, 0.12 ± 0.04 for NGC 6946 X-1, 0.01 ± 0.07 for M82 X-1 and 0.17 ± 0.03 for NGC 1313 X-1 ($1-\sigma$ errors presented).

The ULXs analysed in this paper are very different in spectral hardness (Fig. 4b and 4c). It can be seen in Fig. 4b that the hardness ratios of different sources are correlated with the frequency range in which the QPO appears in a particular source: IC 342 X-1 has the hardest spectrum among the ULXs of our sample and shows the highest QPO frequency (however this source has considerable absorption column, Gladstone et al. 2009; Pintore et al. 2017, which may affect the observed hardness ratio). The softest ULXs, NGC 6946 X-1 and NGC 5408 X-1, show the lowest frequencies, whilst NGC 1313 X-1 having an intermediate hardness shows a QPO at intermediate frequencies. At the same time, the variations of the QPO frequency between different observations of the same ULX almost do not change its spectral hardness. Fitting the hardness-frequency relation using a powerlaw, we obtained indices of 0.02 ± 0.05 for NGC 5408 X-1, 0.047 ± 0.015 for NGC 6946 X-1, 0.01 ± 0.15 and -0.02 ± 0.24 for 32" and 12" apertures of M82 X-1

respectively and -0.002 ± 0.011 for NGC 1313 X-1 ($1-\sigma$ errors). Only the slope of NGC 6946 X-1 is different than zero by more than one sigma. This source shows a weak growth of the hardness with the QPO frequency (Fig. 4b). In the case of NGC 1313 X-1 and IC 342 X-1 the hardness does not change with the QPO frequency, however, it appears to be higher in the brightest observations of these sources where the QPO have not been detected (Fig. 4c).

In transient BHBs the spectral hardness is known to significantly change during an outburst and anti-correlates with the QPO frequency. In other words, a source becomes softer as the frequency increases (Vignarca et al. 2003; Shaposhnikov & Titarchuk 2009). The lack of this correlation in ULXs is one more argument supporting the idea of the difference between sub-Eddington BHBs and ULXs (see Sec. 4).

In the case of M82 X-1 the contaminating flux makes it difficult to determine its true luminosity and hardness. However, despite the contamination, M82 X-1 is an extremely bright ULX reaching an X-ray luminosity of 1.6×10^{41} erg s⁻¹ (Chiang & Kong 2011, from *Chandra* data). Feng & Kaaret (2007) estimated unabsorbed luminosities of 1.3×10^{40} and 1.7×10^{40} erg s⁻¹ for data analysed from ObsIDs 011229020 and 0206080101, respectively. NGC 5408 X-1 had only 7.8×10^{39} erg s⁻¹ during its brightest data set from ObsID 0653380301 (Sutton et al. 2013). Thus, even being relatively faint in the observations presented in Fig. 4a, M82 X-1 remains at least twice brighter than NGC 5408 X-1. However it can not be discarded that the increase of the hardness with the count rate seen in Fig. 4c might be caused by a brightening of the pulsar M82 X-2, which has a hard spectrum (Brightman et al. 2016).

We have considered above only observations with QPO. Although the lack of QPOs in the rest of data sets in some cases might be caused by insufficient exposure time, we did not detect any specific features like flat-topped or power-law noise in their power spectra. The observations without QPO show some power above the level of Poisson noise, however, the shape of their PDS is rather random. For these observations we also calculated the fractional variability (Table 3).

In Fig. 5a we plot the fractional variability (including contribution from both continuum and QPO) versus the rescaled count rate for all analysed observations regardless the presence of the QPO. The F_{rms} is seen to decrease with the apparent luminosity (Fig. 3 and 4a). The absolute rms variability (accounting for the measured noise) also decreases (Fig. 5b). The simultaneous reduction of both quantities indicates that the sources become intrinsically less variable as the luminosities increase. Also Fig. 5b suggests that the linear and positive relation between the absolute rms variability and flux obtained for time scales of a few hours (Heil & Vaughan 2010; Hernández-García et al. 2015) may be violated on longer time scales (months-years).

It is worth to mention that observations with and without QPO form a continuous sequence in Fig. 5 in which the 'lacking-QPO' observations occupy the brightest part of the tail. This may suggest that each source has some luminosity threshold, above which the mechanism producing QPO and FTN breaks down and the variability almost disappears.

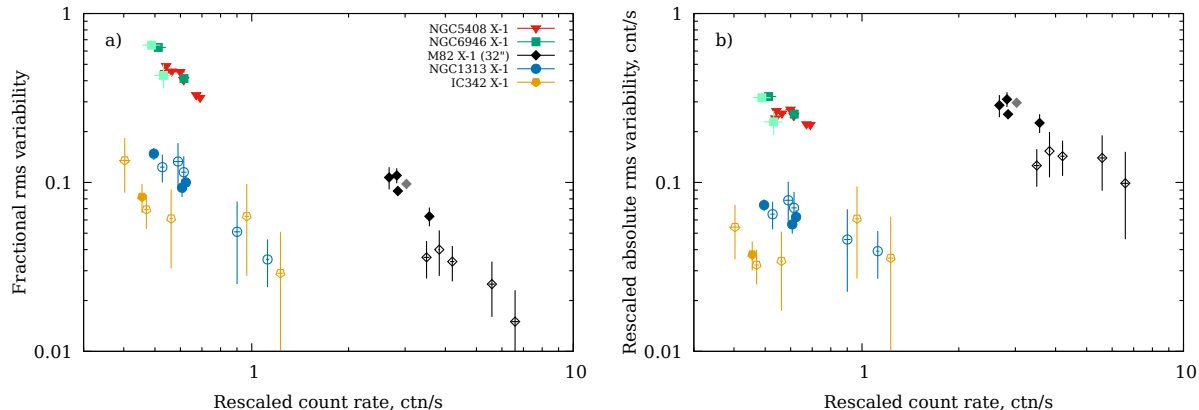


Figure 5. Fractional rms variability (*left panel*) and absolute rms variability (*right panel*) as a function of the count rate. The absolute rms variability and count rates are rescaled to the distance of NGC 5408 X-1. Observations of NGC 6946 X-1 and M82 X-1 where the significance of the QPO is less than 3σ (Table 2) are shown by lighter colours. Observations where we did not detect QPO are indicated by unfilled data points.

4 DISCUSSION

We have carried out a timing analysis of five ULXs that are known to show QPO and have found that their properties are very similar. In each source, the QPO frequency correlates negatively with the fractional rms variability and positively with the apparent luminosity. In general, sources with softer spectra show QPO at lower frequencies, however, a clear correlation between the spectral hardness and QPO frequency has been detected only in the case of NGC 6946 X-1. We also confirmed that the QPO in the PDS always appears together with the FTN.

Sub-Eddington black hole binaries show QPO accompanied by FTN (the so-called type-C QPO) being in their hard intermediate state (Belloni & Motta 2016). Typical frequencies of the type-C QPO observed in stellar mass black holes are between 0.1 and 10 Hz (e.g. GX 339-4 — Motta et al. 2011; XTE J1550-564 — Rao et al. 2010b). It has been proposed that lower QPO frequencies in ULXs may be due to more massive black holes in these systems (Strohmayer & Mushotzky 2009): if the frequency scales inversely proportional to M_{BH} , ULXs should contain black holes with masses of 1000–10000 M_{\odot} (Strohmayer & Mushotzky 2009; Rao et al. 2010a; De Marco et al. 2013). However, the identification of the QPO seen in ULXs with type-C implies that all observed spectral and variability properties must be consistent with the hard intermediate state of BHBs. But this is not the case. It is well-known that the energy spectra of ULXs are not alike the typical for BHBs (Gladstone et al. 2009). The spectra of ULXs when fitted with Comptonization models, yield a thicker and colder Comptonizing medium. The spectral hardness of BHBs is anti-correlated with the QPO frequency (Shaposhnikov & Titarchuk 2009). But in ULXs we have found that the hardness increases with the QPO frequency only in the case of NGC 6946 X-1. The shape of the PDS also differs. In ULXs the QPO peak is located closer to the break (Middleton et al. 2011); we found mean values of $f_q/f_b \sim 3$ in ULXs versus $f_q/f_b \sim 10$ in BHBs (Wijnands & van der Klis 1999). Finally, ULXs show a larger spread of QPO frequencies (with NGC 6946 X-1

having the lowest $f_q \approx 9.4$ mHz versus IC 342 X-1 having the highest $f_q \approx 654$ mHz) which, in the case of the mass scaling argument, would suggest a significant difference in the black hole masses from the ULXs. However, the ULXs analyzed in this paper show a similar behaviour and, probably, have a common underlying super-Eddington accretion nature. Indeed, the discovery of strong relativistic outflows in NGC 5408 X-1 and NGC 1313 X-1 (Pinto et al. 2016) argues in favour of super-Eddington accretion in these sources.

It has been recently shown that some ULXs are pulsating neutron stars. At the moment five ULX pulsars have been found (Bachetti et al. 2014; Fürst et al. 2016; Israel et al. 2017a,b; Kosec et al. 2018). Nevertheless, the analysis of a wide sample of ULXs (including NGC 5408 X-1, M82 X-1 and NGC 1313 X-1) did not detect pulsations (Doroshenko et al. 2015). An explanation for the lack of pulsations has been proposed (Walton et al. 2018), however, we consider it unlikely that all known ULXs eventually will turn out to be neutron stars (King et al. 2001, 2017; Middleton & King 2017). All the ULX pulsars have harder X-ray spectra than what is average in ULXs (Pintore et al. 2017). Many models have been suggested for the ULX-pulsars including magnetic fields of different strengths (Basko & Sunyaev 1976; Mushtukov et al. 2015). One of them requires geometrical beaming in order to violate the Eddington limit (Kawashima et al. 2016).

The structure of supercritical accretion discs was first described by Shakura & Sunyaev (1973). If the matter supply in the outer boundary of the disc significantly exceeds the Eddington rate $\dot{m}_0 = \dot{M}_0/\dot{M}_{Edd} \gg 1$ where $\dot{M}_{Edd} = 48\pi GM/c\kappa$ (assuming a radiative efficiency $\eta = 1/12$) and κ is Thomson opacity, then there is a radius where the force of the radiation pressure becomes equal to the gravity force. This radius is called *spherization radius* and it limits the supercritical area of the disc. Below the spherization radius the disc becomes geometrically thick with $H/R \sim 1$ and it is where the wind is launched. Since the wind possesses an angular momentum, it is supposed to form a funnel with some opening angle. The size of the supercritical area is proportional to the initial accretion rate $R_{sp} = (5/3)\dot{m}_0 R_{in}$ (Poutanen et al. 2007). The inner ra-

dius of the disc R_{in} is usually assumed to be $3R_g$, where $R_g = 2GM/c^2$ is the Schwarzschild radius. Due to the outflow, below R_{sp} the amount of matter accreting through the disc linearly decreases with radius $\dot{m}(R) = \dot{m}_0 \cdot (R/R_{sp})$. This basic concept proposed by Shakura & Sunyaev (1973) and developed in more detail in works by Lipunova (1999) and Poutanen et al. (2007) have been well reproduced by MHD simulations (Ohsuga et al. 2005; Ohsuga & Mineshige 2011).

Below we suggest an interpretation which connects the observed ULX variability properties and the PDS shape in the framework of super-Eddington accretion.

4.1 Lyubarskii's proposal

The variability of X-ray sources is usually interpreted in terms of the mass accretion rate fluctuations arising from random fluctuations of viscosity at different accretion disc radii and propagating inwards. This mechanism was proposed by Lyubarskii (1997) to explain power-law PDS of BHBs. It is supposed that the viscosity varies in all time and spatial scales. The variations of viscosity at one radius change the accretion rate at smaller radii. However, because of the diffusive nature of accretion, only variations on time scales longer than *accretion time* (or *viscosity time*) can propagate whilst the faster variations will be damped. The accretion time increases with radius as:

$$t_a(R) = \left[\alpha \left(\frac{H}{R} \right)^2 \Omega_K(R) \right]^{-1} \quad (2)$$

where α is the viscosity parameter (Shakura & Sunyaev 1973), H is the half-thickness of the disc and Ω_K is the Keplerian frequency; so the outer regions of the disc produce the slowest variations. As the matter passes through the disc, more and more rapid variations are superimposed on these slow ones. Finally, when the matter reaches the inner disc radius, where most of the energy is released, it bears the variations accumulated from all possible disc radii which makes the shape of the resultant PDS power-law. The slope of the PDS is determined by the radial dependence of the amplitude of the viscosity fluctuations. In particular, if the amplitude is the same at all radii then the power spectrum should be $P \propto f^{-1}$.

Uttley & McHardy (2001) have pointed out that additionally to the power-law PDS the mechanism proposed by Lyubarskii also predicts a linear relation between the absolute rms variability and flux, which cannot be explained by other models (for example shot noise model from Terrell 1972). As it latter became clear, the linear rms-flux relation is a very common feature of accreting systems and may be a more fundamental characteristic of the variability than the power spectrum or spectral-timing properties (Uttley et al. 2005). The linear rms-flux relation is observed in binary systems with black holes and neutron stars (Uttley & McHardy 2001; Gleissner et al. 2004; Uttley 2004), active galactic nuclei (Vaughan et al. 2003b, 2005) and cataclysmic variables (Scaringi et al. 2012). This fact made the Lyubarskii's model and its extensions (King et al. 2004; Arévalo & Uttley 2006; Titarchuk et al. 2007; Ingram & Done 2011) very convincing. The discovery of the same behaviour in ULXs (Heil & Vaughan 2010; Hernández-García et al. 2015) sug-

gests that this mechanism must work in these systems as well. Moreover, the Lyubarskii's model was successfully applied to the variability of the supercritical accretion disc of SS433 (Revnivtsev et al. 2006; Atapin et al. 2015; Atapin & Fabrika 2016).

4.2 Flat-topped noise, QPO and spherization radius

Pure power-law PDS predicted by Lyubarskii (1997) for a standard accretion disc can be formed if the accretion time and the fluctuations amplitude smoothly change with radius. In the case of the supercritical disc this is probably not true. Above the spherization radius, where the energy release is not so strong, the structure of the supercritical disc is supposed to be similar to the standard geometrically thin disc with $H/R \sim 0.03 - 0.1$ (Shakura & Sunyaev 1973). But below R_{sp} the disc becomes thick $H/R \sim 1$ (a more precise model including advection, i.e. Lipunova 1999, predicts a disc thickness of 0.6-0.7), which drastically reduces the accretion time. The matter passes a distance from R_{sp} to the innermost orbit almost in the free-fall time. In such a case the spherization radius becomes a trigger, which regulates the matter supply into the supercritical area of the disc. We suppose that if the viscosity at R_{sp} varies in a random and independent manner ("white noise") as it was assumed for all the radii (Lyubarskii 1997), this effect should produce a flat portion in the PDS (Atapin et al. 2015; Middleton et al. 2015b).

In the suggested model the FTN arises from fluctuations occurring at the spherization radius, and the break frequency f_b in the PDS is determined by t_a at R_{sp} . At higher frequencies the power spectrum is related to the fluctuations occurring in the supercritical part of the disc ($R < R_{sp}$). At these frequencies the PDS shape should be power-law as from Lyubarskii (1997), since the accretion time strongly decrease from $t_a(R_{sp})$ to $t_a(R_{in})$. These power-law portions with index β (Table 2) are clearly seen in Fig. 1. Frequencies much lower than the break and FTN should correspond to the subcritical part of the disc ($R \gg R_{sp}$), here the PDS can become power-law again with another (low-frequency) break (Fig. 6). Atapin & Fabrika (2016) discovered such a low-frequency break in SS433 and also found some hints of the power law below 10^{-4} Hz in the ULXs NGC 5408 X-1 and NGC 6946 X-1 (Atapin & Fabrika 2017).

Writing R_{sp} as a function of the initial accretion rate, the break frequency can be estimated as (Hz):

$$f_b \sim t_a^{-1}(R_{sp}) \approx 6.0 \times 10^{-3} \alpha_{0.1} \dot{m}_{300}^{-3/2} m_{10}^{-1} \quad (3)$$

where the disc thickness below R_{sp} is assumed to be $H/R = 0.7$ (Lipunova 1999), $\alpha_{0.1} = \alpha/0.1$, the mass accretion rate \dot{m}_{300} is in units of $300\dot{M}_{Edd}$ and the black hole mass is in units of $10M_\odot$. Using $\dot{M} = 300\dot{M}_{Edd}$, $M_{BH} = 10M_\odot$ and $\alpha = 0.1$, one obtains the break at 6 mHz, the same as observed in NGC 5408 X-1 and NGC 6946 X-1 (Table 2). The accretion rate of $300\dot{M}_{Edd}$ seems reasonable for ULXs because the same value is typical for SS 433 (assuming $M_{BH} \approx 10M_\odot$). Other ULXs showing breaks at higher frequencies may have smaller accretion rates or black hole masses.

The QPO in this model may arise due to instabilities of the accretion flow in the supercritical area of the disc.

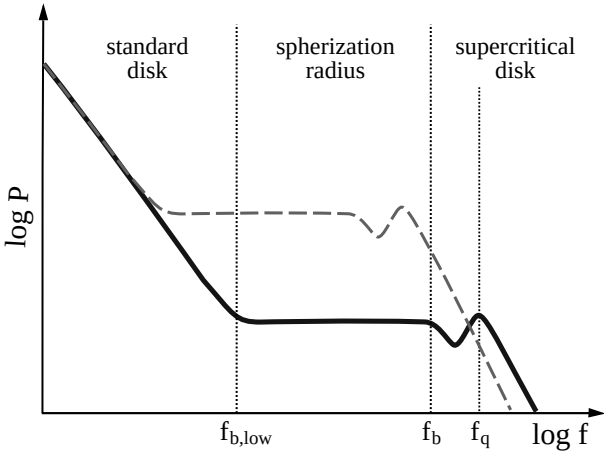


Figure 6. Sketch of the broadband power spectrum of the supercritical accretion disc. Frequencies f_q and f_b mark positions of the QPO and the break observed in ULXs analysed in this work (Fig. 1). The $f_{b,low}$ denotes position of hypothetical low-frequency break lying outside the observable (Atapin & Fabrika 2016, 2017) bandpass. We propose that all three characteristic frequencies are related to the size of the supercritical area of the disc (R_{sp}) which is determined by the accretion rate. The flat-topped noise (FTN) in the PDS occurs due to fluctuations directly at R_{sp} , while the power-law portions $f < f_{b,low}$ and $f > f_b$ originate from the $R \gg R_{sp}$ and $R < R_{sp}$ regions of the disc respectively. As the accretion rate increases, the characteristic frequencies shift toward lower values and the level of FTN becomes higher (power spectrum for the case of higher accretion rate is shown by dashed line).

Below the spherization radius the gravity is dominated by the radiation pressure. The matter is supported by the radiation field; otherwise it could approach the black hole or its surroundings in the free-fall time scale. We suppose that in such a case the QPO frequency may be related to the Keplerian time at the spherization radius:

$$f_q \approx P_K^{-1}(R_{sp}) = \frac{\Omega_K(R_{sp})}{2\pi} \approx 2.0 \times 10^{-2} \dot{m}_{300}^{-3/2} m_{10}^{-1} \quad (4)$$

This formula yields a constant ratio $f_q/f_b = (2\pi(H/R)^2\alpha)^{-1} \sim 3$ (for $H/R = 0.7$ and $\alpha = 0.1$) which is in good agreement with observations (Sec. 3.1). For typical $\dot{M}_0 = 300\dot{M}_{Edd}$ and $M = 10M_\odot$ one obtains $f_q \approx 20$ mHz. QPOs at similar frequencies arising due to instabilities in the supercritical disc have been reproduced in radiation hydrodynamical calculations by Okuda et al. (2009).

4.3 Accretion rates and fractional rms variability

As we have shown in Sec. 3.1, the QPO and break frequencies can vary by 3-5 times between different observations of the same source. We propose that such a behaviour is caused by variations of the initial accretion rate \dot{m}_0 (i.e. accretion rate supplied by the donor star to the outer disc edge). Other parameters like viscosity α , inclination of the super-Eddington disc and opening angle of the wind-funnel (geometrical beaming) may also change and affect the characteristic time scales. To not to complicate the situation with α and all other parameters (which are not understood

yet, but may vary a little) we discuss here only \dot{m}_0 . We propose that the QPO frequency has to be anti-correlated with the accretion rate, i.e. as \dot{m}_0 increases, the spherization radius widens and the QPO and break frequencies decrease. Variations of the QPO frequency by 5 times (in each individual source) imply a variation of the accretion rate by ≈ 3 times. Using eq. (4) and assuming the same black hole mass $M = 10M_\odot$ for all the five ULXs (better estimates for the masses will be discussed below) we estimate \dot{m}_0 as 180–450 for NGC 5408 X-1, 180–520 for NGC 6946 X-1, 90–205 for M 82 X-1, 50–120 for NGC 1313 X-1 and $30\dot{M}_{Edd}$ for IC 342 X-1. If the real masses are lower then the accretion rates need to be higher.

In Sec 3.2 we have shown that the sources become less variable as the QPO frequency increases. We found $F_{rms} \propto f_q^{-\gamma}$ with slopes $\gamma = 0.31 - 0.34$ for NGC 5408 X-1, NGC 6946 X-1, NGC 1313 X-1 and $\gamma \approx 0.17$ for M 82 X-1 (Fig. 3). In the case of IC 342 X-1 there is only one detection of QPO, and it is not possible to determine γ for this ULX. For M 82 X-1 one cannot accurately measure the fractional variability because of the very crowded spatial environment. The real slope of M 82 X-1 could be steeper. Taking this into account we can obtain a relation between the fractional rms variability and the accretion rate: $F_{rms} \propto \dot{m}_0^{0.5}$ (for $\gamma \approx 0.3$).

Such a positive correlation between the fractional variability and the accretion rate is in good agreement with Lyubarskii’s proposal. Also a similar relation between the fractional variability and the break frequency was considered by Middleton et al. (2015a). A major contribution to the F_{rms} is due to the FTN for which its level is expected to depend on the accretion rate. In the model described above and illustrated in Fig. 6 the level of FTN is determined by the low-frequency break $f_{b,low}$. As the accretion rate increases, the supercritical region of the disc increases and the time scales at R_{sp} become longer: Thus the FTN together with QPO and both breaks move upward and to the left in Fig. 6. The total area under the PDS (F_{rms}) also increases. When the \dot{m}_0 decreases, the FTN goes to in the opposite direction and the F_{rms} decreases.

In Fig. 5a we show the fractional variability of the observations where we did not detect QPO. In this figure the observations with and without QPO form a single sequence in which the ‘QPO-less’ observations show lower F_{rms} . This fact may imply that the accretion rate in the ‘QPO-less’ observations is significantly lower. We suggest that only NGC 5408 X-1 and NGC 6946 X-1 from the list of the five ULXs considered here have higher \dot{m}_0 because in these sources we always see a QPO (if one includes two observations of NGC 6946 X-1 where the QPO is only marginally detected). In other ULXs (NGC 1313 X-1, M 82 X-1 and IC 342 X-1) the QPO disappears at higher frequencies when \dot{m}_0 and F_{rms} decrease. Using observations with the lowest F_{rms} (Table 3) and the relation $F_{rms} \propto \dot{m}_0^{0.5}$ we can estimate the lowest accretion rate for NGC 1313 X-1, M 82 X-1 and IC 342 X-1 as 7.1, 2.6 and 3.8 \dot{M}_{Edd} respectively. However, these values might be underestimated. This result depends on the black hole mass. Nevertheless, in these three ULXs the QPO may disappear when accretion rate falls below some critical level.

In the following we explain the possible reasons for the presence of QPOs and FTN in the power spectra of only a few (five) ULXs but not in others. In Table 2 we see

that the QPO peak becomes broader as the frequency increases (Fig. 2). It is common for Lorentzian components that with increasing frequency the FWHM must increase as well (Belloni et al. 2002). We suggest that QPOs might disappear because of the broadening. Therefore, if \dot{m}_0 reduces then the QPO peak moves to higher frequencies, it broadens and disappears. Having a low enough accretion rate may be the reason of not observing FTN and QPO in some well-known ULXs. Through the study of the PDS of 16 sources, a sample of ULXs with low variability has been revealed by Heil et al. (2009). More observations are needed to confirm that other ULXs really do not have QPOs, since the five ULXs with QPO studied here have been observed during long exposures.

4.4 X-ray luminosity, spectral hardness and suggested black hole masses

We found that the observed X-ray luminosity slightly increases with the QPO frequency (Fig. 4a) as $L_X \propto f_q^{0.16 \pm 0.04}$ (for NGC 5408 X-1, Sec. 3.2). Taking into account the relation (4) of f_q and \dot{m}_0 , it would result into a negative correlation between the accretion rate and luminosity. On the other hand, the bolometric luminosity of the super-Eddington accretion disc should increase with higher accretion rate (Shakura & Sunyaev 1973; Poutanen et al. 2007; assuming the beaming factor equal to unity):

$$L_X = L_{Edd}(\ln \dot{m}_0 + 1) \quad (5)$$

We suppose that there is no conflict between observations and theory here. Part of the X-ray radiation originating from the innermost regions of the funnel must be scattered or absorbed in the wind. The stronger the outflow, the more the X-ray photons will be scattered. Since most of the matter supplied to the disc by the donor star is eventually ejected from the system (Shakura & Sunyaev 1973; Poutanen et al. 2007), then the mass loss rate in the wind \dot{m}_w has to be strongly dependent on \dot{m}_0 . When \dot{m}_0 increases, the logarithmic factor $\ln \dot{m}_0$ has to increase, but the X-ray luminosity cannot overcome the scattering in the wind. Of course, it could depend on other parameters (for example, beaming), however, this may complicate the situation.

Using the observed luminosities we can estimate the black hole masses because the X-ray luminosity in eq. (5) is proportional to L_{Edd} which scales with the mass. The result might be affected by \dot{m}_0 through both the logarithmic factor and the scattering of X-ray photons in the wind. Therefore, we used only the brightest observation in Table 1 and Fig. 5 for each ULX to reduce uncertainties due to scattering. Expressing the masses in units of the mass from the BH in NGC 5408 X-1, one obtains 0.9, 9.5, 1.6 and 1.8 for NGC 6946 X-1, M 82 X-1, NGC 1313 X-1 and IC 342 X-1 respectively. So, all the ULXs except M 82 X-1 have similar masses. It is clear that more accurate assessments should also consider other parameters, namely beaming and inclination. Moreover in the case of NGC 5408 X-1 and NGC 6946 X-1 luminosities and masses might be underestimated because in these sources we see QPO even in the brightest observations and the scattering may be significant.

The spectral hardness also can depend on accretion rate. In Fig. 4b we showed that the sources show very different hardness, and that it correlates with the frequency

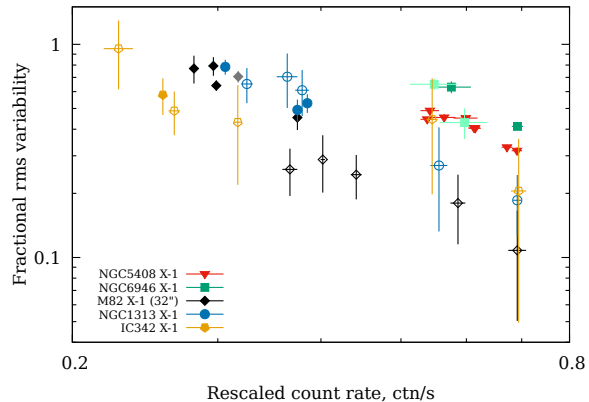


Figure 7. Similar to Fig. 5a but accounted for the difference in the accretion rate and black hole mass between the sources. The distances, masses and accretion rates are rescaled to those that in NGC 5408 X-1. The legend is the same as in Fig. 3. Observations without QPO are shown by unfilled data points. Lighter colours denotes observations of NGC 6946 X-1 and M 82 X-1 with the QPO significance less than 3σ .

of the QPO appears in each source. The hardest one is IC 342 X-1 (Shidatsu et al. 2017) having the highest QPO frequency and, probably, the lowest accretion rate. The softest ones, NGC 5408 X-1 and NGC 6946 X-1 show the lowest QPO frequencies and seem to have the highest accretion rate. This could imply that the hardness increases as the accretion rate decreases. This effect might be due to, for example, the optically thick wind which having a relatively soft spectrum (Poutanen et al. 2007) may cover the innermost hottest regions of the accretion disk emitting hard X-rays (Middleton et al. 2011; Sutton et al. 2013). Nevertheless, it is still unclear why the hardness does not change with the QPO frequency. We found small changes only in NGC 6946 X-1 (Fig. 4b). However in the brightest observations of NGC 1313 X-1, IC 342 X-1 and M 82 X-1 (without QPO, Fig. 4c) the hardness appears to be higher. Also we do not understand why NGC 5408 X-1 and NGC 6946 X-1 differ in hardness, despite they have similar accretion rate and masses. It might be related to different black hole spin or orientation of the systems but we do not consider these parameters for simplicity. The effect of inclination on spectral hardness is discussed in Middleton et al. (2015b).

In Fig. 7 we show the fractional rms variability versus the rescaled count rate similar to Fig. 5a but corrected for the difference in the black hole mass and accretion rate. Both quantities are rescaled to NGC 5408 X-1. To recalculate the luminosity we used the masses obtained above and eq. (5). For the fractional variability we used the relation $F_{rms} \propto f_q^{-\gamma}$ with $\gamma \approx 0.31$ for NGC 6946 X-1, $\gamma \approx 0.17$ for M 82 X-1 and $\gamma \approx 0.34$ for NGC 1313 X-1 and IC 342 X-1. In Fig. 7 the ULXs become much closer than they are in Fig. 5a, especially M 82 X-1, NGC 1313 X-1 and IC 342 X-1. However, some differences between the sources in this figure still remain. It is possible that other parameters, that we did not take into account, are important.

Obviously, this interpretation is just a suggestion; the masses from all ULXs can depend on other parameters like beaming, orientation, etc. Furthermore, the wind itself may produce the variability (Middleton et al. 2011, 2015b) which

makes the picture much more complicated. We only follow what Shakura & Sunyaev (1973) and Lyubarskii (1997) found in order to explain the behaviour of the observed variability from ULXs. Those studies allowed us to connect the flat-topped noise, QPO, F_{rms} , luminosity and spectral hardness with the spherization radius and accretion rate.

5 CONCLUSIONS

In this paper we have analyzed the power spectra of five ULXs that are known to show considerable amount of fast variability and QPO. We found that, despite the fact that ULXs significantly differ in the spectral hardness and QPO frequencies, their variability properties are quite similar. In all the cases the QPO is accompanied by flat-topped noise whose level is anti-correlated with the QPO frequency. As the frequency increases, the sources become brighter and less variable.

We propose that this behaviour can be explained in terms of supercritical accretion from Shakura & Sunyaev (1973) and propagating fluctuations from Lyubarskii (1997). Most of the observed variability properties are governed by the accretion rate which regulates the size of the supercritical area of the disc (spherization radius). Both QPO and FTN are related to the accretion time at R_{sp} . As the accretion rate increases, the spherization radius increases and the FTN and QPO move toward lower frequencies and upwards. The level of FTN as well as the fractional variability increase. The outflow from the disc also increases, which makes the apparent X-ray luminosity lower due to scattering in the wind. In opposite situation, when we do not observe the QPO and FTN, the \dot{m}_0 might be too small (but anyway super-Eddington). This could be the reason why one cannot observe QPO in other ULXs.

We infer that NGC 5408 X-1, NGC 6946 X-1, NGC 1313 X-1 and IC 342 X-1 may contain black holes of similar masses, whilst the black holes in M82 X-1 may be ≈ 10 times more massive. From the QPO frequencies we conclude that the highest accretion rates are found in NGC 5408 X-1 and NGC 6946 X-1 ($\sim 200 - 500 \dot{M}_{Edd}$) and the lowest in IC 342 X-1 ($\sim 30 \dot{M}_{Edd}$). In the case of observations where QPO have not been detected, the accretion rate may be even lower.

ACKNOWLEDGEMENTS

We thank the anonymous referee for careful reading of the paper and useful remark. This work is based on the data from the *XMM-Newton*, an ESA Science Mission with instruments and contributions directly funded by ESA member states and the USA (NASA). The research was supported by the Russian RFBR grants 18-32-20214, 19-02-00432. MCG acknowledges support provided by the European Seventh Frame-work Programme (FP7/2007-2013) under grant agreement n° 312789 and GA CR grant 18-00533S and also funding from ESA through a partnership with IAA-CSIC (Spain).

REFERENCES

- Agrawal V. K., Nandi A., 2015, *MNRAS*, 446, 3926
 Arévalo P., Uttley P., 2006, *MNRAS*, 367, 801
 Atapin K. E., Fabrika S. N., 2016, *Astronomy Letters*, 42, 517
 Atapin K., Fabrika S., 2017, in Balega Y. Y., Kudryavtsev D. O., Romanyuk I. I., Yakunin I. A., eds, *Stars: From Collapse to Collapse Vol. 510 of Astronomical Society of the Pacific Conference Series, Flat Power Spectra of Ultraluminous X-ray Sources: Evidence of Super-Eddington Accretion*. p. 478
 Atapin K., Fabrika S., Medvedev A., Vinokurov A., 2015, *MNRAS*, 446, 893
 Bachetti M. et al., 2013, *ApJ*, 778, 163
 Bachetti M. et al., 2014, *Nature*, 514, 202
 Bachetti M., 2016, *Astronomische Nachrichten*, 337, 349
 Barnard R., Trudolyubov S., Haswell C. A., Kolb U. C., Osborne J. P., Priedhorsky W. H., 2007, in di Salvo T., Israel G. L., Piersant L., Burderi L., Matt G., Tornambe A., Menna M. T., eds, *The Multicolored Landscape of Compact Objects and Their Explosive Origins Vol. 924 of American Institute of Physics Conference Series, Artificial variability in XMM-Newton observations of X-ray sources: M31 as a case study*. pp 691–696
 Basko M. M., Sunyaev R. A., 1976, *MNRAS*, 175, 395
 Belloni T. M., Motta S. E., 2016, in Bambi C., ed., *Astrophysics of Black Holes: From Fundamental Aspects to Latest Developments Vol. 440 of Astrophysics and Space Science Library, Transient Black Hole Binaries*. p. 61
 Belloni T., Psaltis D., van der Klis M., 2002, *ApJ*, 572, 392
 Brightman M., Harrison F., Walton D. J., Fuerst F., Hornschemeier A., Zezas A., Bachetti M., Grefenstette B., Ptak A., Tendulkar S., Yukita M., 2016, *ApJ*, 816, 60
 Caballero-García M. D., Belloni T. M., Wolter A., 2013a, *MNRAS*, 435, 2665
 Caballero-García M. D., Belloni T., Zampieri L., 2013b, *MNRAS*, 436, 3262
 Cherepashchuk A., 2002, *Space Sci. Rev.*, 102, 23
 Cherepashchuk A. M., Postnov K. A., Belinski A. A., 2018, *MNRAS*, 479, 4844
 Chiang Y.-K., Kong A. K. H., 2011, *MNRAS*, 414, 1329
 Colbert E. J. M., Mushotzky R. F., 1999, *ApJ*, 519, 89
 De Marco B., Ponti G., Miniutti G., Belloni T., Cappi M., Dadina M., Muñoz-Darias T., 2013, *MNRAS*, 436, 3782
 Dewangan G. C., Griffiths R. E., Rao A. R., 2006, *ApJL*, 641, L125
 Dheeraj P. R., Strohmayer T. E., 2012, *ApJ*, 753, 139
 Doroshenko V., Santangelo A., Ducci L., 2015, *A&A*, 579, A22
 Edelson R., Turner T. J., Pounds K., Vaughan S., Markowitz A., Marshall H., Dobbie P., Warwick R., 2002, *ApJ*, 568, 610
 Fabrika S., 2004, *ASPRv*, 12, 1
 Fabrika S., Mescheryakov A., 2001, in Schilizzi R. T., ed., *Galaxies and their Constituents at the Highest Angular Resolutions Vol. 205 of IAU Symposium, Face-on SS 433 stars as a possible new type of extragalactic X-ray sources*. p. 268
 Fabrika, S. N., Abolmasov, P. K., Karpov, S., 2007, in Karas V. and Matt G., eds, *Black Holes from Stars to Galaxies – Across the Range of Masses IAU Symposium*

- N 238, The supercritical accretion disk in SS 433 and ultraluminous X-ray sources/ p. 225
- Fabrika S., Ueda Y., Vinokurov A., Sholukhova O., Shidatsu M., 2015, *Nature Physics*, 11, 551
- Feng H., Kaaret P., 2007, *ApJ*, 668, 941
- Feng H., Rao F., Kaaret P., 2010, *ApJL*, 710, L137
- Fürst F. et al., 2016, *ApJL*, 831, L14
- Gleissner T., Wilms J., Pottschmidt K., Uttley P., Nowak M. A., Staubert R., 2004, *A&A*, 414, 1091
- Gladstone J. C., Roberts T. P., Done C., 2009, *MNRAS*, 397, 1836
- Heil L. M., Vaughan S., 2010, *MNRAS*, 405, L86
- Heil L. M., Vaughan S., Roberts T. P., 2009, *MNRAS*, 397, 1061
- Hernández-García L., Vaughan S., Roberts T. P., Middleton M., 2015, *MNRAS*, 453, 2877
- Ingram A., Done C., 2011, *MNRAS*, 415, 2323
- Israel G. L. et al., 2017a, *MNRAS*, 466, L48
- Israel G. L. et al., 2017b, *Science*, 355, 817
- Kaaret P., Feng H., Roberts T. P., 2017, *ARA&A*, 55, 303
- Kawashima T., Mineshige S., Ohsuga K., Ogawa T., 2016, *PASJ*, 68, 83
- King A. R., Pringle J. E., West R. G., Livio M., 2004, *MNRAS*, 348, 111
- King A., Lasota J.-P., Kluźniak W., 2017, *MNRAS*, 468, L59
- King A. R., Davies M. B., Ward M. J., Fabbiano G., Elvis M., 2001, *ApJL*, 552, L109
- Kosec P., Pinto C., Walton D. J., Fabian A. C., Bachetti M., Brightman M., Fürst F., Grefenstette B. W., 2018, *MNRAS*, 479, 3978
- Lipunova G. V., 1999, *Astronomy Letters*, 25, 508
- Lyubarskii Y. E., 1997, *MNRAS*, 292, 679
- Matsumoto H., Tsuru T. G., Koyama K., Awaki H., Canizares C. R., Kawai N., Matsushita S., Kawabe R., 2001, *ApJL*, 547, L25
- McClintock J. E., Remillard R. A., 2006, *Black hole binaries*. pp 157–213
- Medvedev A., Fabrika S., 2010, *MNRAS*, 402, 479
- Middleton M. J., King A., 2017, *MNRAS*, 470, L69
- Middleton M. J., Roberts T. P., Done C., Jackson F. E., 2011, *MNRAS*, 411, 644
- Middleton M. J., Walton D. J., Roberts T. P., Heil L., 2014, *MNRAS*, 438, L51
- Middleton M. J., Walton D. J., Fabian A., Roberts T. P., Heil L., Pinto C., Anderson G., Sutton A., 2015a, *MNRAS*, 454, 3134
- Middleton M. J., Heil L., Pintore F., Walton D. J., Roberts T. P., 2015b, *MNRAS*, 447, 3243
- Middleton M. J. et al., 2018, *arXiv:1810.10518*
- Motta S., Muñoz-Darias T., Casella P., Belloni T., Homan J., 2011, *MNRAS*, 418, 2292
- Mushtukov A. A., Suleimanov V. F., Tsygankov S. S., Poutanen J., 2015, *MNRAS*, 447, 1847
- Ohsuga K., Mineshige S., 2011, *ApJ*, 736, 2
- Ohsuga K., Mori M., Nakamoto T., Mineshige S., 2005, *ApJ*, 628, 368
- Okuda T., Lipunova G. V., Molteni D., 2009, *MNRAS*, 398, 1668
- Pasham D. R., Strohmayer T. E., 2013, *ApJ*, 771, 101
- Pasham D. R., Cenko S. B., Zoghbi A., Mushotzky R. F., Miller J., Tombesi F., 2015, *ApJL*, 811, L11
- Pinto C., Middleton M. J., Fabian A. C., 2016, *Nature*, 533, 64
- Pinto C., Alston W., Soria R., Middleton M. J., Walton D. J., Sutton A. D., Fabian A. C., Earnshaw H., Urquhart R., Kara E., Roberts T. P., 2017, *MNRAS*, 468, 2865
- Pintore F., Zampieri L., Wolter A., Belloni T., 2014, *MNRAS*, 439, 3461
- Pintore F., Zampieri L., Stella L., Wolter A., Mereghetti S., Israel G. L., 2017, *ApJ*, 836, 113
- Poutanen J., Lipunova G., Fabrika S., Butkevich A. G., Abolmasov P., 2007, *MNRAS*, 377, 1187
- Protassov R., van Dyk D. A., Connors A., Kashyap V. L., Siemiginowska A., 2002, *ApJ*, 571, 545
- Rao F., Belloni T., Stella L., Zhang S. N., Li T., 2010b, *ApJ*, 714, 1065
- Rao F., Feng H., Kaaret P., 2010a, *ApJ*, 722, 620
- Revnivtsev M. et al., 2006, *A&A*, 447, 545
- Roberts T. P., 2007, *Ap&SS*, 311, 203
- Scaringi S., Körding E., Uttley P., Groot P. J., Knigge C., Still M., Jonker P., 2012, *MNRAS*, 427, 3396
- Shakura N. I., Sunyaev R. A., 1973, *A&A*, 24, 337
- Shaposhnikov N., Titarchuk L., 2009, *ApJ*, 699, 453
- Shidatsu M., Ueda Y., Fabrika S., 2017, *ApJ*, 839, 46
- Stobart A.-M., Roberts T. P., Wilms J., 2006, *MNRAS*, 368, 397
- Strohmayer T. E., Mushotzky R. F., 2003, *ApJL*, 586, L61
- Strohmayer T. E., Mushotzky R. F., 2009, *ApJ*, 703, 1386
- Strohmayer T. E., Mushotzky R. F., Winter L., Soria R., Uttley P., Cropper M., 2007, *ApJ*, 660, 580
- Sutton A. D., Roberts T. P., Middleton M. J., 2013, *MNRAS*, 435, 1758
- Takeuchi S., Ohsuga K., Mineshige S., 2013, *PASJ*, 65
- Takeuchi S., Ohsuga K., Mineshige S., 2014, *PASJ*, 66, 48
- Terrell Jr. N. J., 1972, *ApJL*, 174, L35
- Tikhonov N. A., 2014, *Astronomy Letters*, 40, 537
- Tikhonov N. A., Galazutdinova O. A., 2010, *Astronomy Letters*, 36, 167
- Tikhonov N. A., Galazutdinova O. A., 2016, *Astronomy Letters*, 42, 428
- Titarchuk L., Shaposhnikov N., Arefiev V., 2007, *ApJ*, 660, 556
- Tully R. B. et al., 2013, *AJ*, 146, 86
- Uttley P., 2004, *MNRAS*, 347, L61
- Uttley P., McHardy I. M., 2001, *MNRAS*, 323, L26
- Uttley P., McHardy I. M., Vaughan S., 2005, *MNRAS*, 359, 345
- van der Klis M., 1997, *Statistical Challenges in Modern Astronomy*, Vol II. Springer-Verlag., p. 321
- Vaughan S., Fabian A. C., Nandra K., 2003b, *MNRAS*, 339, 1237
- Vaughan S., Edelson R., Warwick R. S., Uttley P., 2003a, *MNRAS*, 345, 1271
- Vaughan S., Iwasawa K., Fabian A. C., Hayashida K., 2005, *MNRAS*, 356, 524
- Vignarca F., Migliari S., Belloni T., Psaltis D., van der Klis M., 2003, *A&A*, 397, 729
- Vikhlinin A., Churazov E., Gilfanov M., 1994, *A&A*, 287, 73
- Walton D. J. et al., 2014, *ApJ*, 793, 21
- Walton D. J. et al., 2018, *ApJ*, 856, 128
- Wijnands R., van der Klis M., 1999, *ApJ*, 514, 939